Journal of proteome research

Article

Proteomic profiling suggests central role of STAT signaling during retinal degeneration in the rd10 mouse model

Alice Ly, Juliane Merl-Pham, Markus Priller, Fabian Gruhn, Nicole Senninger, Marius Ueffing, and Stefanie M Hauck

J. Proteome Res., **Just Accepted Manuscript** • DOI: 10.1021/acs.jproteome.6b00111 • Publication Date (Web): 04 Mar 2016

ACS Publications

Journal of Proteome Research is published by the American Chemical Society. 1155 Sixteenth Street N.W., Washington, DC 20036

Proteomic profiling suggests central role of STAT signaling during retinal degeneration in the *rd10* mouse model

Running title: Proteomic profiling of retinal degeneration

Alice Ly [1,2]‡, *Juliane Merl-Pham*[1]‡, *Markus Priller*[1], *Fabian Gruhn*[1], *Nicole Senninger*[1], *Marius Ueffing*[1,3], *Stefanie M. Hauck*[1]*

[1]Research Unit Protein Science, Helmholtz Zentrum München, German Research Center for Environmental Health (GmbH), Neuherberg, Germany.

[2] Research Unit Analytical Pathology, Helmholtz Zentrum München, German Research Center for Environmental Health (GmbH), Neuherberg, Germany.

[3]Centre of Ophthalmology, Institute for Ophthalmic Research, University of Tübingen, Tübingen, Germany.

‡These authors contributed equally.

Corresponding Author

* Stefanie M. Hauck, Research Unit Protein Science, Helmholtz Zentrum München, German Research Center for Environmental Health (GmbH), Ingolstaedter Landstr.1, 85764 Munich/Neuherberg

Telephone: +49-89-3187-3941

Email: hauck@helmholtz-muenchen.de

ABSTRACT

The *rd10* mouse is a model of retinitis pigmentosa characterized by the dysfunction of a rod-photoreceptor-specific phosphodiesterase. Compared to the *rd1* mouse, retinal degeneration in the *rd10* mouse begins later in age with a milder phenotype, making it ideal for investigating cell death and neuroprotective mechanisms. Alterations in the *rd10* retina proteome at pre-, peak-, and post-degenerative time points were examined using a modified high-recovery filter-aided sample preparation (FASP) method in combination with label-free quantitative mass spectrometry, generating a proteomic dataset on almost 3000 proteins. Our data confirmed a period of protein expression similar to age-matched wild-type mice pre-degeneration, with decreases in proteins associated with phototransduction and increases in signaling proteins at peak- and post-degenerative stages. 57 proteins were differentially expressed in the *rd10* retinae during peak-degeneration compared to wild-type mice after stringent FDR correction ($q<0.05$). Network analysis separated these proteins into a cluster of downregulated photoreceptor proteins, and one of upregulated signaling proteins centered around GFAP, STAT3, and STAT1. This is the first study to identify alterations in STAT1 in the *rd10* mouse, which were confirmed with gene expression and immunoblotting experiments underpinning the efficacy of our approach. This unique proteomic dataset on protein dynamics during retinal degeneration could serve as an information source for vision research in the future.

KEYWORDS

Label-free mass spectrometry

phospho-STAT

Retinal Müller glial cells

Immunohistochemistry

Eye

Retinitis pigmentosa

Photoreceptor cell death

INTRODUCTION

Retinitis pigmentosa (RP) is an umbrella term for inherited degenerative eye diseases that are typically characterized by photoreceptor death leading to decreased visual fields, night blindness, and eventually legal or complete blindness. Over 180 different genes causing inherited retinal diseases have been mapped.[1] Mutations in the β subunit of rod cGMP phosphodiesterase (*PDE6B*) cause an autosomal recessive form of RP characterized by degeneration of rod photoreceptors which account for approximately 4% of retinitis pigmentosa cases.[2] Mutations in the mouse analogue, *Pde6b*, similarly cause retinal degenerative diseases in mice, and provide a useful model to examine the pathogenesis of RP.

The most commonly studied mouse model of *Pde6b* retinal degeneration is the *rd1* mutant.[3] The *rd1* mutation is found in many different laboratory mice strains and is caused by a nonsense point mutation in exon 7 and viral insert in intron -1 of the *Pde6b* gene resulting in a non-functional protein.[3–5] This results in a very fast degeneration with rod cell death beginning around post-natal day (PN)10, peaking around PN14, and is complete by the third week of life.[6] Despite the mutation being only present in rod photoreceptors, all retinal cells respond to the degeneration with reactive gliosis seen by the increase of glial fibrillary acidic protein (GFAP) in Müller cells, inner retinal synaptic remodeling following rod degeneration, and cone photoreceptor death.[7–9] However, the speed of the degeneration and the early age at which it begins in the *rd1* mouse can lead to challenges in interpreting the pathological degenerative mechanisms as it overlaps with a period of developmental apoptosis.

Another *Pde6b* mutant, the *rd10* mouse, contains a missense mutation in exon 13, resulting in a partially functioning gene and slower rate of degeneration compared to *rd1* mice.[10,11] Retinal development in *rd10* mice is normal at two weeks of age.[11–13] Following this, rod photoreceptors rapidly degenerate with peak death rates at PN21;[13] by the fourth week of age, the outer nuclear layer (ONL) is reduced to only a few rows of cells corresponding primarily

to cone photoreceptors.[11,12] Like *rd1* mice, significant synaptic remodeling, vascular changes, and gliosis occur in *rd10* mice following photoreceptor degeneration.[11–14] Unlike *rd1* mutants, the slower rate of degeneration in the *rd10* results in a period where the retina is physiologically functional, as detected through the electroretinogram (ERG),[11,12] although these responses are slower and decreased compared to mice with normal vision. Given that retinal structure and function are maintained for longer and the degeneration does not overlap with developmental apoptosis, the *rd10* mouse is a superior RP model for examining the progression of degenerative pathways. In addition, as the *rd10* mutation spontaneously arose in C56Bl/6 mice,[10] these mice serve as an appropriate wild-type. In comparison, while the C3H/HeH mouse line used as a control for *rd1* studies has forced expression of wild-type *Pde6b* and normal retinal histology, ERG recordings from this strain are decreased compared to wild-type BALB/c mice.[15]

This study investigates protein alterations at significant time points in the *rd10* retina with label-free quantitative mass spectrometry. Samples were prepared using a filter-associated sample preparation (FASP) protocol.[16] FASP has been demonstrated on a variety of tissues such as liver,[16] aorta,[17] and brain,[18] and is particularly efficient at identifying a large number of proteins from samples containing small numbers of cells,[19] which makes this approach ideal for small organs such as mouse retina. Using hierarchical clustering and network analysis, we identified an increasing number of differentially abundant proteins at the degenerative PN21 and PN28 timepoints, which were then validated by qPCR, immunofluorescence and western-blot.

EXPERIMENTAL SECTION

Animals

Mice (wild-type [C57Bl/6N] and *rd10* [B6.CXB1-*Pde6b*^{rd10}/J]; Jackson Laboratories, Bar Harbor, ME, USA) were bred and maintained at a constant temperature (22 ± 1°C), with a 12:12 hour light:dark cycle and free access to food and water. Male mice were sacrificed at PN14, PN21, and PN28 via cervical dislocation. The eyes were immediately enucleated, and the retina either completely dissected free from the eye, frozen in liquid nitrogen, and stored at -80°C for until further processing, or the cornea, lens, and vitreous removed with the posterior eyecup fixed in 4% paraformaldehyde in 0.1M phosphate buffer for 30 minutes and processed for histology.[20] All procedures adhered to the ARVO guidelines of the Use of Animals in Ophthalmic and Vision Research.

Filter-Aided Sample Preparation

Samples were prepared using a modified Filter Aided Sample Preparation (FASP) protocol.[16] Retina samples (n=4 per age and mouse strain) were lysed in buffer A (9 M urea, 2 M thiourea, 4% CHAPS, 65 mM DTT), and homogenized for two 30 second cycles at 65000 rpm with a 20 second pause between each cycle using the Precellys Ceramic Kit (Peqlab Biotechnologie, Erlangen, Germany). Following homogenization, samples were incubated at room temperature, centrifuged for 3 minutes at 17,500 *g*, supernatants transferred to LoBind tubes (Eppendorf, Hamburg, Germany), and the protein content determined using a Bradford assay. Samples were later used for LC-MS/MS and Western Blot (WB) analysis. For mass spectrometric analysis, 10µg of each sample was diluted 1:10 in 50mM ammoniumbicarbonate and incubated with 10µl 100mM dithiothreitol for 30 minutes at 60ºC. Samples were alkylated with 10 µl of 300 mM iodoacteamide at room temperature in the dark, and then pipetted onto a 30 kD centrifuge filter (Pall Corporation,

NY, USA). Following centrifugation at 14,000 *g*, the flowthrough was discarded and the remaining sample repeatedly washed with UA buffer (8 M urea in 0.1 M Tris/HCl, pH 8.5), followed by 50 mM ammonium bicarbonate (ABC) with the flowthrough discarded between washes. The samples were diluted again in ABC, then proteolysed on the filter with 1µg Lys-C (Wako) for 2 hours at room temperature, and proteolysed with trypsin (Promega) at 37ºC overnight. The samples were centrifuged at 15,000 *g* for 15 min through the filter and the flowthrough added to fresh LoBind tubes. The filter was washed with 50 mM ABC/2% acetonitrile (ACN), centrifuged at 15,000 *g* for 15 min and the flowthrough pooled with the flowthrough obtained in the prior step. Trifluoracetic acid (TFA; pH 2) was added to the samples prior to LC-MS/MS analysis.

Mass Spectrometry

LC-MS/MS analysis was performed as described previously on an LTQ OrbitrapXL (Thermo Fisher Pierce).[21,22] Before loading, samples were centrifuged for 5 min at 4 ºC. Approximately 0.5 µg of each sample was automatically loaded onto the trap column at a flow rate of 30 µl/min in 97% buffer A (2% ACN/3%DMSO/0.1% formic acid (FA)) and 3% buffer B (73 % ACN/3% DMSO/0.1 % FA in HPLC-grade water).[23] After 5 min, the peptides were eluted, and separated at 300 nl/min flow rate on the analytical column by a 140 min gradient from 3 to 35% of buffer B, followed by a short gradient from 35% to 95% buffer B in 5 min. The gradient was reset back to 3% buffer B and left to equilibrate for 20 min between each sample. From the MS prescan, the 10 most abundant peptide ions were selected for fragmentation in the linear ion trap if they were at least doubly charged and if they exceeded an intensity of at least 200 counts, with a dynamic exclusion of 60 seconds. During fragment analysis, a high-resolution (60,000 full width at half-maximum) MS spectrum was acquired with a mass range from 300 to 1500 Da.

Label-Free Analysis

The acquired spectra of the different samples were loaded and analyzed using Progenesis LC-MS software (Version 2.5, Nonlinear Dynamics) for label-free quantification as previously described.[21] The profile data of the MS scans were transformed into peak lists with respective *m/z* values, intensities, abundances, and *m/z* width. MS/MS spectra were treated similarly. Using the most complex sample as reference, the retention times of the other samples were aligned by automatic alignment to a maximal overlay of the 2D features. Features with one or more than seven charges were excluded from further analyses. Samples were then allocated to their respective experimental and age groups.

All MS/MS spectra were exported as Mascot generic files (mgf) and used for peptide identification with Mascot (version 2.4) using the Ensembl Mouse protein database (*mus musculus*; release 72, 51765 sequences, 23352282 residues). Search parameters used were 10ppm peptide mass tolerance, 0.6 Da fragment mass tolerance, one missed cleavage allowed, carbamidomethylation was set as fixed modification, and methionine oxidation and deamidation of asparagine and glutamine were allowed as variable modifications. Mascot integrated decoy database search was set to a false discovery rate (FDR) of 1% when searching was performed on the concatenated mgf files with a percolator ion score cut-off of 15 and an appropriate significance threshold p. Identifications were re-imported into Progenesis LC-MS. For quantification, only unique peptides of an identified protein were included and the total cumulative normalized abundance was calculated by summing the abundances of all peptides allocated to the respective protein. No minimal thresholds were set for the method of peak picking or selection of data to use for quantifications. This study utilized proteins identified and quantified by at least one peptide with a mascot percolator score of $\geq$ 15 for further analysis. A t-test implemented in the Progenesis QI software

comparing the normalized abundances of the individual proteins between groups was calculated and corrected for multiple testing resulting in q-values (FDR adjusted p-values) given in supplemental tables 1 to 4. Furthermore a ratio average (*rd10*/wild-type) was calculated for each time point.

The mass spectrometry proteomics data have been deposited to the ProteomeXchange Consortium [24] via the PRIDE partner repository with the dataset identifier PXD002584.

Cluster, Protein Network and Pathway Enrichment Analysis

Protein clusters, interaction maps and pathway enrichment analysis was conducted using 57 proteins significantly different at P21 ($q < 0.05$).

Cluster analysis of the P14, P21 and P28 $\log_2$ transformed *rd10*/wildtype ratios was performed using Cluster 3.0 software.[25] The observed ratios were normalised and the distance matrix calculated using the 'Euclidean distance' setting. Hierarchical clustering was completed using the 'complete linkage' algorithm for comparison of the behaviour of the individual proteins at different timepoints. The resultant tree and heatmap were visualised with Java Treeview (http://www.eisenlab.org/eisen/?page_id=42).

For protein map generation, corresponding gene names and fold changes were uploaded into Genomatix Pathway System (GePS, http://www.genomatix.de, Genomatix), and created using *Mus musculus* as the organism with literature mining conducted at the function word level. All unconnected proteins were removed from the network; upregulated proteins colored yellow and downregulated proteins were colored blue.

Pathway enrichment analysis was performed with Generanker (http://www.genomatix.de, Genomatix) again using *Mus musculus* as organism. For the determination of enriched molecular functions, clusters A+B and cluster E (see figure 2) were processed separately.

Significantly enriched molecular function assignments were exported and are displayed in supplemental tables 6 and 7.

mRNA isolation and cDNA generation.

Total RNA was isolated from wild-type and *rd10* retinae at P14 and P21 (n=3/age).[26] Retinae were homogenized in 750 µl TRIzol (Invitrogen, Karlsruhe) and incubated for 5 minutes at room temperature. 150 µl of chloroform was then added to the sample and agitated for 15 seconds, incubated for 3 minutes, and centrifuged (4°C, 15 minutes, maximum speed). The supernatant was transferred to a new microcentrifuge tube with 375 µl of isopropanol, incubated for 10 minutes at room temperature, and centrifuged (4°C, 10 minutes, maximum speed). The pellet was washed with 75% ethanol and treated with RQ1 RNase-free DNase Kit (Promega, WI, USA) to eliminate contaminating genomic DNA. Total RNA samples were quantified using a Nanodrop (Thermo Fisher Scientific). cDNA was then generated using the Fermentas RevertAid First Strand cDNA Synthesis Kit (Thermo Fisher Scientific) following the producer's instructions. To improve yield, oligo$(dT)_{20}$-Primers together with random hexamer primers were used for synthesis.

Relative Quantification with qRT-PCR

Quantitative real-time PCR was performed with a LightCycler 480-System (Roche Diagnostics, Mannheim, Germany) using a commercially available reaction mixture, KAPA SYBR FAST qPCR MasterMix for Roche Light Cycler480 (Peqlab, Erlangen, Germany). Reactions were carried out in triplicate. Relative gene expression levels were determined by normalization to the expression level of the housekeeping gene hypoxantine guanine phosphoribosyl transferase 1 (*Hprt1*). The delta delta C_t method was used to calculate fold

expression levels.[27] See supplementary table 5 for primer sequences. The number of independent replicates was n=4 for all genes, except for *Stat1* (n=2).

Immunofluorescence and Microscopy

After fixation in 4% paraformaldehyde and cryoprotection in graded (10%, 20%, and 30%) sucrose, eyecups were dissected, embedded and vertically sectioned (12 μm, Microm560 cryostat). For examining morphology, sections were washed with 0.1M phosphate buffer (PB), and stained with DAPI. Immunofluorescence was performed as described previously.[20] Briefly, sections were blocked (10% normal goat serum, 1% bovine serum albumin, and 0.5% Triton X-100 in PB) for 1 hour, and for single staining incubated overnight in rabbit anti-GFAP antibody (1:10,000, #Z0334, Dako) diluted in 3% normal goat serum, 1% bovine serum albumin, and 0.5% Triton X-100 in PB. After rinsing, sections were incubated in goat anti-rabbit 488 secondary antibody (1:1000, AlexaFluor, Invitrogen) for 90 minutes, counterstained (Hoechst 1:5000, #H3570, Molecular Probes), rinsed in PB, and coverslipped.

For double staining after blocking, sections were incubated overnight in rabbit anti-STAT1 antibody (1:500, #HPA000982, Sigma) diluted in 3% normal goat serum, 1% bovine serum albumin, and 0.5% Triton X-100 in PB. After rinsing, sections were incubated in goat anti-rabbit 488 secondary antibody (1:1000, AlexaFluor, Invitrogen) for 90 minutes, followed by another overnight incubation in mouse anti-glutamine synthetase (1:1000, #610517, BD Transduction Labs) diluted in 3% normal goat serum, 1% bovine serum albumin, and 0.5% Triton X-100 in PB and incubation in goat anti-mouse 568 secondary antibody (1:1000, AlexaFluor, Invitrogen) for 90 minutes. After counterstaining (Hoechst 1:5000, #H3570, Molecular Probes) and rinsing in PB the sections were coverslipped.

Sections were photographed on an AxioImager Z1 with ApoTome attachment (Zeiss) with constant variables maintained for each section.

Western Blot (WB) Analysis

The levels of STAT1, STAT3, and phosphorylated STAT1 and STAT3 in the WT or *rd10* lysates were determined in WBs using 15µg of tissue lysate, with alpha-tubulin as a loading control. Blots were blocked in 3% BSA in 1xTBST for 1h at room temperature and incubated overnight in rabbit anti-STAT1 (1:500; #HPA000982, Sigma), rabbit anti-pSTAT1 (Ser-727, 1:1000; #8826, Cell signaling), rabbit anti-STAT3 (1:1000; #4904, Cell signaling), rabbit anti-pSTAT3 (1:1000; #9145, Cell signaling), or rat anti-alpha tubulin (1:10,000; #AB6160, Abcam,). Species appropriate secondary HRPO-coupled antibodies were used in a dilution of 1:10,000. Protein signals were visualized using ECL Plus enhanced chemiluminescence kit (GE Healthcare) and quantified using ImageJ.

Statistical Analysis

Proteomics data were analysed using the *t*-test function in Progenesis QI (two sided, unpaired), followed by correction for multiple testing, with resulting p- and q-values given in supplemental tables 2 to 4.

The qPCR results are plotted using GraphPad Prism5 (GraphPad Software) and expressed as mean ± SEM.

RESULTS

Time course of photoreceptor degeneration

To confirm previous studies that reported normal retinal morphology in two week old *rd10* mice, rod degeneration at three weeks and completion by four weeks of age,[11–13] peripheral retinal sections from wild-type and *rd10* were stained with DAPI at PN14, PN21 and PN28 (figure 1). Peripheral retina was chosen as it is reported to degenerate more slowly than central retina.[12] In accordance with these studies, the photoreceptor nuclei-containing outer nuclear layer in PN14 wild-type (figure 1A) and *rd10* (figure 1B) are of comparable size. At PN21, the *rd10* ONL is approximately half the size of wild-type ONL (figure 1C-D), and is reduced to one layer of nuclei by PN28 (figure 1E-F).

Proteomic profiling of retina at different time-points during degeneration.

Retinal proteins were extracted from complete tissue at PN14, PN21, and PN28 and mass spectrometric samples were prepared using FASP. FASP has been demonstrated as a method that allows the efficient analysis of samples consisting of a small number of cells,[16,19] and is therefore appropriate for an organ such as mouse retina. Combining the results of the three time points, we identified a total of 2885 different proteins and a total of 2620 proteins were quantified (supplemental table 1), with an overall coefficient of variation between replicates of 27% indicating high reproducibility of the performed workflow. Using the average normalized abundances, a *t*-test with subsequent correction for multiple testing and the ratio of *rd10* versus wild-type for each time point were calculated to determine which proteins were significantly different between the animal groups and the degree of the alteration. A volcano plot comparing individual protein significance q-values against corresponding ratios indicate a close scatter at P14 that increases by PN21, with the widest distribution at PN28 (supplemental figure 1). These results indicate that only few proteins are differentially

abundant at PN14, prior to overt degeneration, but that this number increases with age and degenerative time course.

Protein networks affected by retinal degeneration

At PN14, which is considered the time point preceding obvious retinal degeneration, only 2 proteins were significantly differentially abundant between *rd10* and wildtype retinae based on FDR-adjusted q values (q<0.05), including PDE6G (supplemental table 2). In contrast, most differences in expression were detected at PN28 (1359 significantly different proteins with q<0.05, supplementary table 4), as expected, since this time point reflects advanced degeneration. We considered the proteins significantly altered at PN21 the most interesting set, because this time point corresponds to peak degeneration in *rd10* mice and consequently used this set for interaction and pathway enrichment analysis. 57 proteins were significantly different at PN21 after correction for multiple testing (q < 0.05), of which 25 and 32 were up- and downregulated respectively (supplemental table 3).

Hierarchical clustering was conducted for these proteins using their respective fold-changes between wild-type and *rd10* mutant at PN14, 21, and 28 to further examine alterations in protein levels and determine whether this was reflective of functional alterations during disease progression (figure 2). From this, five clusters were identified corresponding to ratio expression behavior. Clusters A and B are comprised of proteins with decreased abundances, with cluster A having peak difference at PN28, and cluster B peaking at PN21. Cluster C consists of proteins that displayed decreased ratios at PN21 and increased at PN28; this was reversed for the proteins in cluster D. Cluster E contains proteins with peak increased abundances at PN21 or PN28.

To investigate whether these groupings are also reflective of functional similarity, the clusters were analyzed for overrepresentation of specific molecular function assignments with

Generanker pathway enrichment analysis. Clusters A and B were combined as they followed the same abundance trends. Cluster E was analyzed separately. Clusters C and D were not analysed with Generanker as they only consisted of a small numbers of proteins making pathway analyses difficult to perform and interpret.

Analysis of combined cluster A and B indicated that down-regulated proteins are overwhelmingly associated with phototransduction processes (supplemental table 6). These proteins also formed the core of the down-regulated sub-network in the Genomatix interaction map shown in figure 3, indicating a large degree of overlap between the two analyses.

In contrast, the proteins in cluster E were associated with protein binding, chemokine and cytokine signaling (supplemental table 7). Most interesting molecular functions were chemokine receptor binding processes involving STAT1 and STAT3, which also form part of the larger sub-network in figure 3.

A protein interaction map was generated using Genomatix Pathway System GePS (Genomatix) to identify functional protein networks (figure 3). The map indicated one large network, consisting of two sub-networks, one of which is composed of downregulated proteins involved in rod photoreceptor function and structure, such as the phosphodiesterase subunits PDE6B, PDE6A, and PDE6G, cyclic nucleotide-gated channels CNGA1 and CNGB1, and rod outer membrane protein (ROM1). The other sub-network consists of a core of upregulated cell signaling proteins, such as Signal Transducer and Activator of Transcription 1 and 3 (STAT1, STAT3), Guanylate Binding Protein 2, Interferon-Inducible (GBP2) and Vascular Cell Adhesion Molecule 1 (VCAM1), surrounded by their modulation targets.

Validation of PN21 proteomic alterations via immunofluorescence, qPCR and western blot

Immunofluorescence was conducted on PN21 tissue to determine the anatomical location of alterations in GFAP and STAT1 levels. At PN21, GFAP expression is only found in the ganglion cell layer (GCL) of the wild-type retina, but is expressed in retinal Müller glial processes reaching into remains of the outer nuclear layer (ONL) in *rd10* retina (figure 4A). Immunoreactivity of STAT1 antibody was elevated in the *rd10* retina compared to PN21 wild-type retina (figure 4B). While STAT1 is increased overall in the *rd10* retina, the labelling in the inner plexiform and ganglion cell layers appears to localize to Müller cell processes. Double immunofluorescence for STAT1 and glutamine synthetase for Müller cells confirmed this, as double labelling was absent in the age-matched control (figure 4B).

The gene expressions of *Pdea6a*, *Slc24a1, Mvp, Stat3, Stat1* and *Gfap* were further examined based on the cluster, network and pathway analyses. Figure 4C is a comparison of the measured gene expression fold changes to the corresponding proteomic values. The qPCR results confirmed those found by the proteomic screen – candidates with decreased protein abundances had decreased gene expression and those with increased abundances had increased gene expression.

Having confirmed alterations in STAT1 via immunofluorescence and qPCR, and STAT3 with qPCR, the total protein and corresponding phosphorylation states were examined with western blots. Figure 4D not only confirms an increase in STAT1 and STAT3 levels, but also reveals increased pSTAT1 and pSTAT3 relative to loading control (tubulin). Interestingly, total STAT1 levels were increased approximately 2-fold and pSTAT1 levels even more than 5-fold, whereas total STAT3 levels were increased 4-fold and pSTAT3 levels only 3-fold.

DISCUSSION

This study utilized label-free quantitative mass spectrometry to investigate changes in the retinal proteome at three significant time points in a mouse model of retinitis pigmentosa. Using a highly reproducible and sensitive sample preparation protocol, the *rd10* model of photoreceptor degeneration was examined at 2, 3, and 4 weeks of age, which respectively correspond to pre-, peak-, and post-degenerative time points. Correspondingly, we found the greatest number of alterations occurred at PN21 and 28. Furthermore, concentrating on the PN21 timepoint indicated particular changes not just in proteins associated with visual transduction and retinal function, but also the signaling proteins STAT1 and STAT3. Alterations in the levels of these proteins were confirmed at the gene expression and anatomic level.

Although the *rd10* mouse model of retinal degeneration is not as well studied as mice with the *rd1* mutation, it is potentially a better model to investigate degenerative processes and sight-restorative therapies as the slow rate of degeneration confers a period of visual functionality in *rd10* mice.[11,12,28,28] Perhaps the most important difference between the *rd1* and *rd10* models is that the later commencement of pathologic cell death in the *rd10* does not overlap with the developmental apoptosis. Therefore, any detected pathways would only be due to degenerative processes.

This is the first study to examine *rd10* disease progression using a proteomics approach. Studies using targeted or untargeted proteomic screens and network analysis have been successfully used to examine protein changes and identify potential biomarkers in other retinal diseases. We have previously used proteomics approaches to identify autoantigens and the upregulation of pro-inflammatory proteins in equine recurrent uveitis,[21,22,29] and examined the effect of anti-hyperglycaemic treatment on the retinal membrane proteome of a mouse model of type 2 diabetes.[30] 2D-gel-based proteomic analyses of the *rd1* mouse retina have

identified an increase in crystallins in parallel with a decrease in rod proteins,[31] and increased phosphorylation of phosducin and activation of calcium/calmodulin-activated protein kinase II.[32] In contrast to the aforementioned studies of *rd1* retinas, we have used here a LC-MS/MS-based proteomic approach applying a FASP protocol due to its reported higher sensitivity and suitability for small sample amounts compared to other preparation methods.[19] The sensitivity of this approach is reflected in the high protein yield from our samples, with an approximately 3 to 5 fold increase in identification rates in comparison to several other proteomic analyses of mammalian retinas. [21,30,33] Furthermore, our results reflect what is known of *rd10* progression as well as enabling identification of a new signaling pathway in this disease. In agreement with the described proteomic changes in retinal degeneration in the *rd1* mutant, we found rod proteins downregulated and GFAP heavily upregulated at PN21 and PN28. Altogether we could identify eight crystallins in our dataset, of which some were up- and some were down-regulated in the *rd10* mutant, most of them without reaching significance (supplemental table 1). Furthermore we found COP9 homolog subunit 8 significantly upregulated at PN28 ($q<0.05$) in agreement with previous data on the *rd1* mutant.[32] Both recoverin and phosducin were significantly altered at PN28 (and even PN21 for phosducin), as described before for the *rd1* mutant. [31,32]

The window of relatively normal visual function in *rd10* mice can be interpreted from our proteomic results. Significant differences in protein abundance and fold change are primarily apparent from PN21 onwards while levels at PN14 are similar to the wild-type, confirming that this is indeed a pre-degenerative timepoint. Hierarchical clustering and network analysis showed that downregulated proteins at PN21 and PN28 are primarily associated with phototransduction, which is consistent with the degenerative time course in *rd10* mice, as peak rod degeneration occurs at PN21, and is fully complete at PN28.[10,13]

Interestingly Related RAS Viral (R-Ras) Oncogene Homolog (RRAS) was highly downregulated both at PN28 and PN21 with q-values of 0.006 and 0.085 respectively. Although considered an oncogene, RRAS protein expression in normal tissues is found on endothelium and differentiated smooth muscle cells.[34] RRAS expression in the retina has not been thoroughly investigated but the association of RRAS with vascular tissues is in line with a previous study in which RRAS was identified via microarray as significantly altered in rodent models of retinal neovascularization.[35] Loss of blood vessels following the onset of degeneration has been described to occur in rd10 mice,[36] which is likely the reason for the decrease in RRAS abundance.

Pathway analysis of differentially abundant proteins at PN21 produced a network of proteins that were upregulated at this degenerative timepoint and centered around transcription factors Signal Transducer and Activator of Transcription-1 (STAT1) and STAT3, and intermediate filament Glial Fibrillary Acidic Protein (GFAP). GFAP is a marker of gliosis and is upregulated in macroglial Müller cells in many retinal diseases including *rd10*.[7,11,13,20,29,37] In this study, increased GFAP was detected at the protein and gene expression level from PN21, with labelled sections showing the characteristic increase in Müller cell processes. The role of gliosis in disease promotion or attenuation is contentious as the cells undergo significant changes, some of which can be neuroprotective or detrimental, such as the release of neurotrophic factors or formation of a glial scar.[38] While the exact role of gliosis in retinal degeneration remains to be elucidated, a recent study found that IGF-1 treatment in *rd10* mice decreased Müller cell gliosis and photoreceptor death.[39] Also increased at PN21 is phospholipase C, beta 4 (PLBC4), which is also linked to STAT1 and STAT3 and has a role in modulating visual response.[40]

Our proteomic screen found increases in both STAT1 and STAT3 which was confirmed at the mRNA level for both proteins and via immunohistochemistry for STAT1. Although the

proteomics analysis does not allow for assignment of altered protein abundances to certain cell types within a complex tissue like the retina, immunohistochemistry of tissue sections allows for correlation of protein changes to individual tissue regions and cell types, like demonstrated here for altered STAT1 levels in Müller cells.

Western blots not only confirmed the total protein changes, but also increases in STAT1 and STAT3 phosphorylation, indicative of signaling activation. STAT3 signaling has been demonstrated to be neuroprotective to photoreceptors,[41] post-photoreceptoral neurons,[42] and the retinal pigment epithelium,[43] and has therefore been much studied in the context of different models of retinal degeneration. The upregulation of STAT3 protein and associated genes were found to be increased in a mouse model of cone degeneration, particularly within Müller glia cells.[44] Upregulation of STAT3 also occurred in a zebrafish model of light-induced degeneration and shown to be required for Müller cell proliferation.[45] In contrast, light damage in a mouse model showed only a slight change in STAT3 over time, although a strong increase in the active phosphorylated form (pSTAT3) occurred following light exposure.[46] This same group examined STAT3 and pSTAT3 in *rd10* mice, finding increased STAT3 gene expression and phosphorylation from PN21 to PN56.[13] In contrast to our results, western blots for total STAT3 protein levels do not appear altered, however western blotting is not as sensitive and quantitative as mass spectrometry.[47]

We have shown previously unreported increases in STAT1 gene expression, total protein, and phosphorylated protein levels in *rd10* retina at PN21. Alterations in STAT1 in the degenerative retina have been less reported overall compared to STAT3. While total STAT1 protein is reported as being elevated in *rd1* retina compared to wild-type animals, pSTAT1 levels were not altered.[46] Experiments using ciliary neurotrophic factor (CNTF) stimulation have been conflicting with respect to STAT1 activation. Peterson *et al*. found intravitreal injections of the CNTF analog axokine into healthy Sprague-Dawley rats dramatically

increased total STAT1 but had a weak and delayed effect on pSTAT1 levels.[48] Additionally, while light stimulation dramatically increased total STAT1 levels, pSTAT1 was only slightly affected [48]. In comparison, continuous CNTF expression following viral insertion increased expression and phosphorylation of both STAT1 and STAT3 in mice with a slow retinal degeneration genotype.[49] It is likely that the varying responses of STAT1 and STAT3 and their phosphorylated forms between degenerative models are due to differences in the mechanisms of damage and neuroprotection.

CONCLUSIONS

In summary, this study demonstrates the viability of mass spectrometric analysis in the investigation of retinal degenerations. Our results indicate that there is a period where retinal protein abundances of *rd10* mice are comparable to those found in wild-type mice, followed by a period of degeneration from the third week of life. Once degeneration begins, there is a massive decrease in proteins associated with transduction, reflective of the loss of photoreceptor cells, and a concomitant upregulation of signaling proteins. In particular, we confirmed the previously unreported upregulation of STAT1 through qPCR and immunofluorescence. These findings add to our understanding of protein alterations and signaling processes occurring in retinal degeneration. Furthermore our unique proteomic dataset provides useful information on the behavior of almost 3000 proteins during retinal degeneration and could serve as an information source for other scientists in vision research in future.

REFERENCES

(1) Daiger, S. P.; Bowne, S. J.; Sullivan, L. S. Perspective on genes and mutations causing retinitis pigmentosa. *Arch. Ophthalmol.* **2007**, *125*, 151–158.

(2) McLaughlin, M. E.; Ehrhart, T. L.; Berson, E. L.; Dryja, T. P. Mutation spectrum of the gene encoding the beta subunit of rod phosphodiesterase among patients with autosomal recessive retinitis pigmentosa. *Proc. Natl. Acad. Sci. U.S.A.* **1995**, *92*, 3249–3253.

(3) Chang, B.; Hawes, N. L.; Hurd, R. E.; Davisson, M. T.; Nusinowitz, S.; Heckenlively, J. R. Retinal degeneration mutants in the mouse. *Vision Res.* **2002**, *42*, 517–525.

(4) Bowes, C.; Li, T.; Danciger, M.; Baxter, L. C.; Applebury, M. L.; Farber, D. B. Retinal degeneration in the rd mouse is caused by a defect in the beta subunit of rod cGMP-phosphodiesterase. *Nature* **1990**, *347*, 677–680.

(5) Bowes, C.; Li, T.; Frankel, W. N.; Danciger, M.; Coffin, J. M.; Applebury, M. L.; Farber, D. B. Localization of a retroviral element within the rd gene coding for the beta subunit of cGMP phosphodiesterase. *Proc. Natl. Acad. Sci. U.S.A.* **1993**, *90*, 2955–2959.

(6) Sancho-Pelluz, J.; Arango-Gonzalez, B.; Kustermann, S.; Romero, F. J.; van Veen, T.; Zrenner, E.; Ekström, P.; Paquet-Durand, F. Photoreceptor cell death mechanisms in inherited retinal degeneration. *Mol. Neurobiol.* **2008**, *38*, 253–269.

(7) Chua, J.; Nivison-Smith, L.; Fletcher, E. L.; Trenholm, S.; Awatramani, G. B.; Kalloniatis, M. Early remodeling of Müller cells in the rd/rd mouse model of retinal dystrophy. *J. Comp. Neurol.* **2013**, *521*, 2439–2453.

(8) Punzo, C.; Cepko, C. Cellular responses to photoreceptor death in the rd1 mouse model of retinal degeneration. *Invest. Ophthalmol. Vis. Sci.* **2007**, *48*, 849–857.

(9) Strettoi, E.; Pignatelli, V. Modifications of retinal neurons in a mouse model of retinitis pigmentosa. *Proc. Natl. Acad. Sci. U.S.A.* **2000**, *97*, 11020–11025.

(10) Chang, B.; Hawes, N. L.; Pardue, M. T.; German, A. M.; Hurd, R. E.; Davisson, M. T.; Nusinowitz, S.; Rengarajan, K.; Boyd, A. P.; Sidney, S. S.; et al. Two mouse retinal degenerations caused by missense mutations in the beta-subunit of rod cGMP phosphodiesterase gene. *Vision Res.* **2007**, *47*, 624–633.

(11) Gargini, C.; Terzibasi, E.; Mazzoni, F.; Strettoi, E. Retinal organization in the retinal degeneration 10 (rd10) mutant mouse: a morphological and ERG study. *J. Comp. Neurol.* **2007**, *500*, 222–238.

(12) Barhoum, R.; Martínez-Navarrete, G.; Corrochano, S.; Germain, F.; Fernandez-Sanchez, L.; de la Rosa, E. J.; de la Villa, P.; Cuenca, N. Functional and structural modifications during retinal degeneration in the rd10 mouse. *Neuroscience* **2008**, *155*, 698–713.

(13) Samardzija, M.; Wariwoda, H.; Imsand, C.; Huber, P.; Heynen, S. R.; Gubler, A.; Grimm, C. Activation of survival pathways in the degenerating retina of rd10 mice. *Exp. Eye Res.* **2012**, *99*, 17–26.

(14) Phillips, M. J.; Otteson, D. C.; Sherry, D. M. Progression of neuronal and synaptic remodeling in the rd10 mouse model of retinitis pigmentosa. *J. Comp. Neurol.* **2010**, *518*, 2071–2089.

(15) Hoelter, S. M.; Dalke, C.; Kallnik, M.; Becker, L.; Horsch, M.; Schrewe, A.; Favor, J.; Klopstock, T.; Beckers, J.; Ivandic, B.; et al. "Sighted C3H" mice--a tool for analysing the influence of vision on mouse behaviour? *Front. Biosci.* **2008**, *13*, 5810–5823.

(16) Wiśniewski, J. R.; Zougman, A.; Nagaraj, N.; Mann, M. Universal sample preparation method for proteome analysis. *Nat. Methods* **2009**, *6*, 359–362.

(17) Kaga, E.; Karademir, B.; Baykal, A. T.; Ozer, N. K. Identification of differentially expressed proteins in atherosclerotic aorta and effect of vitamin E. *J Proteomics* **2013**, *92*, 260–273.
(18) Nepomuceno, A. I.; Gibson, R. J.; Randall, S. M.; Muddiman, D. C. Accurate identification of deamidated peptides in global proteomics using a quadrupole orbitrap mass spectrometer. *J. Proteome Res.* **2014**, *13*, 777–785.
(19) Wiśniewski, J. R.; Ostasiewicz, P.; Mann, M. High recovery FASP applied to the proteomic analysis of microdissected formalin fixed paraffin embedded cancer tissues retrieves known colon cancer markers. *J. Proteome Res.* **2011**, *10*, 3040–3049.
(20) Ly, A.; Yee, P.; Vessey, K. A.; Phipps, J. A.; Jobling, A. I.; Fletcher, E. L. Early inner retinal astrocyte dysfunction during diabetes and development of hypoxia, retinal stress, and neuronal functional loss. *Invest. Ophthalmol. Vis. Sci.* **2011**, *52*, 9316–9326.
(21) Hauck, S. M.; Dietter, J.; Kramer, R. L.; Hofmaier, F.; Zipplies, J. K.; Amann, B.; Feuchtinger, A.; Deeg, C. A.; Ueffing, M. Deciphering Membrane-Associated Molecular Processes in Target Tissue of Autoimmune Uveitis by Label-Free Quantitative Mass Spectrometry. *Molecular & Cellular Proteomics* **2010**, *9*, 2292–2305.
(22) Merl, J.; Deeg, C. A.; Swadzba, M. E.; Ueffing, M.; Hauck, S. M. Identification of Autoantigens in Body Fluids by Combining Pull-Downs and Organic Precipitations of Intact Immune Complexes with Quantitative Label-Free Mass Spectrometry. *J. Proteome Res.* **2013**.
(23) Hahne, H.; Pachl, F.; Ruprecht, B.; Maier, S. K.; Klaeger, S.; Helm, D.; Médard, G.; Wilm, M.; Lemeer, S.; Kuster, B. DMSO enhances electrospray response, boosting sensitivity of proteomic experiments. *Nat. Methods* **2013**, *10*, 989–991.
(24) Vizcaíno, J. A.; Deutsch, E. W.; Wang, R.; Csordas, A.; Reisinger, F.; Ríos, D.; Dianes, J. A.; Sun, Z.; Farrah, T.; Bandeira, N.; et al. ProteomeXchange provides globally coordinated proteomics data submission and dissemination. *Nat. Biotechnol.* **2014**, *32*, 223–226.
(25) Eisen, M. B.; Spellman, P. T.; Brown, P. O.; Botstein, D. Cluster analysis and display of genome-wide expression patterns. *Proc. Natl. Acad. Sci. U.S.A.* **1998**, *95*, 14863–14868.
(26) Chomczynski, P. A reagent for the single-step simultaneous isolation of RNA, DNA and proteins from cell and tissue samples. *BioTechniques* **1993**, *15*, 532–534, 536–537.
(27) Livak, K. J.; Schmittgen, T. D. Analysis of relative gene expression data using real-time quantitative PCR and the 2(-Delta Delta C(T)) Method. *Methods* **2001**, *25*, 402–408.
(28) Thomas, B. B.; Shi, D.; Khine, K.; Kim, L. A.; Sadda, S. R. Modulatory influence of stimulus parameters on optokinetic head-tracking response. *Neurosci. Lett.* **2010**, *479*, 92–96.
(29) Hauck, S. M.; Schoeffmann, S.; Amann, B.; Stangassinger, M.; Gerhards, H.; Ueffing, M.; Deeg, C. A. Retinal Mueller glial cells trigger the hallmark inflammatory process in autoimmune uveitis. *J. Proteome Res.* **2007**, *6*, 2121–2131.
(30) Ly, A.; Scheerer, M. F.; Zukunft, S.; Muschet, C.; Merl, J.; Adamski, J.; Hrabě de Angelis, M.; Neschen, S.; Hauck, S. M.; Ueffing, M. Retinal proteome alterations in a mouse model of type 2 diabetes. *Diabetologia* **2013**.
(31) Cavusoglu, N.; Thierse, D.; Mohand-Saïd, S.; Chalmel, F.; Poch, O.; Van-Dorsselaer, A.; Sahel, J.-A.; Léveillard, T. Differential proteomic analysis of the mouse retina: the induction of crystallin proteins by retinal degeneration in the rd1 mouse. *Mol. Cell Proteomics* **2003**, *2*, 494–505.

(32) Hauck, S. M.; Ekström, P. A. R.; Ahuja-Jensen, P.; Suppmann, S.; Paquet-Durand, F.; van Veen, T.; Ueffing, M. Differential modification of phosducin protein in degenerating rd1 retina is associated with constitutively active Ca2+/calmodulin kinase II in rod outer segments. *Mol. Cell Proteomics* **2006**, *5*, 324–336.

(33) Cao, L.; Wang, L.; Cull, G.; Zhou, A. Alterations in molecular pathways in the retina of early experimental glaucoma eyes. *Int J Physiol Pathophysiol Pharmacol* **2015**, *7*, 44–53.

(34) Komatsu, M.; Ruoslahti, E. R-Ras is a global regulator of vascular regeneration that suppresses intimal hyperplasia and tumor angiogenesis. *Nat. Med.* **2005**, *11*, 1346–1350.

(35) Recchia, F. M.; Xu, L.; Penn, J. S.; Boone, B.; Dexheimer, P. J. Identification of genes and pathways involved in retinal neovascularization by microarray analysis of two animal models of retinal angiogenesis. *Invest. Ophthalmol. Vis. Sci.* **2010**, *51*, 1098–1105.

(36) Otani, A.; Dorrell, M. I.; Kinder, K.; Moreno, S. K.; Nusinowitz, S.; Banin, E.; Heckenlively, J.; Friedlander, M. Rescue of retinal degeneration by intravitreally injected adult bone marrow-derived lineage-negative hematopoietic stem cells. *J. Clin. Invest.* **2004**, *114*, 765–774.

(37) Downie, L. E.; Pianta, M. J.; Vingrys, A. J.; Wilkinson-Berka, J. L.; Fletcher, E. L. Neuronal and glial cell changes are determined by retinal vascularization in retinopathy of prematurity. *J. Comp. Neurol.* **2007**, *504*, 404–417.

(38) Bringmann, A.; Iandiev, I.; Pannicke, T.; Wurm, A.; Hollborn, M.; Wiedemann, P.; Osborne, N. N.; Reichenbach, A. Cellular signaling and factors involved in Müller cell gliosis: neuroprotective and detrimental effects. *Prog Retin Eye Res* **2009**, *28*, 423–451.

(39) Arroba, A. I.; Alvarez-Lindo, N.; van Rooijen, N.; de la Rosa, E. J. Microglia-Müller glia crosstalk in the rd10 mouse model of retinitis pigmentosa. *Adv. Exp. Med. Biol.* **2014**, *801*, 373–379.

(40) Jiang, H.; Lyubarsky, A.; Dodd, R.; Vardi, N.; Pugh, E.; Baylor, D.; Simon, M. I.; Wu, D. Phospholipase C beta 4 is involved in modulating the visual response in mice. *Proc. Natl. Acad. Sci. U.S.A.* **1996**, *93*, 14598–14601.

(41) von Toerne, C.; Menzler, J.; Ly, A.; Senninger, N.; Ueffing, M.; Hauck, S. M. Identification of a novel neurotrophic factor from primary retinal Muller cells using SILAC. *Mol. Cell Proteomics* **2014**.

(42) Lin, P.-K.; Ke, C.-Y.; Khor, C. N.; Cai, Y.-J.; Lee, Y.-J. Involvement of SDF1a and STAT3 in granulocyte colony-stimulating factor rescues optic ischemia-induced retinal function loss by mobilizing hematopoietic stem cells. *Invest. Ophthalmol. Vis. Sci.* **2013**, *54*, 1920–1930.

(43) Patel, A. K.; Hackam, A. S. Toll-like receptor 3 (TLR3) protects retinal pigmented epithelium (RPE) cells from oxidative stress through a STAT3-dependent mechanism. *Mol. Immunol.* **2013**, *54*, 122–131.

(44) Schaeferhoff, K.; Michalakis, S.; Tanimoto, N.; Fischer, M. D.; Becirovic, E.; Beck, S. C.; Huber, G.; Rieger, N.; Riess, O.; Wissinger, B.; et al. Induction of STAT3-related genes in fast degenerating cone photoreceptors of cpfl1 mice. *Cell. Mol. Life Sci.* **2010**, *67*, 3173–3186.

(45) Nelson, C. M.; Gorsuch, R. A.; Bailey, T. J.; Ackerman, K. M.; Kassen, S. C.; Hyde, D. R. Stat3 defines three populations of Müller glia and is required for initiating maximal müller glia proliferation in the regenerating zebrafish retina. *J. Comp. Neurol.* **2012**, *520*, 4294–4311.

(46) Samardzija, M.; Wenzel, A.; Aufenberg, S.; Thiersch, M.; Remé, C.; Grimm, C. Differential role of Jak-STAT signaling in retinal degenerations. *FASEB J.* **2006**, *20*, 2411–2413.

(47) Aebersold, R.; Burlingame, A. L.; Bradshaw, R. A. Western Blots versus Selected Reaction Monitoring Assays: Time to Turn the Tables? *Mol Cell Proteomics* **2013**, *12*, 2381–2382.

(48) Peterson, W. M.; Wang, Q.; Tzekova, R.; Wiegand, S. J. Ciliary neurotrophic factor and stress stimuli activate the Jak-STAT pathway in retinal neurons and glia. *J. Neurosci.* **2000**, *20*, 4081–4090.

(49) Rhee, K. D.; Ruiz, A.; Duncan, J. L.; Hauswirth, W. W.; Lavail, M. M.; Bok, D.; Yang, X.-J. Molecular and cellular alterations induced by sustained expression of ciliary neurotrophic factor in a mouse model of retinitis pigmentosa. *Invest. Ophthalmol. Vis. Sci.* **2007**, *48*, 1389–1400.

ACKNOWLEDGMENT

The authors would like to thank Jacob Menzler for participating in the animal breeding and Sandra Helm and Silke Becker for excellent technical assistance.

This work was supported by the Ministry of Education and Research of the Federal Republic of Germany (BMBF) grant numbers 0315505A (SysTec-Verbund IMAGING), and 01GM1108A (HOPE II – FKZ).

AUTHOR CONTRIBUTION

The manuscript was written through contributions of all authors. All authors have given approval to the final version of the manuscript.

CONFLICT OF INTEREST DISCLOSURE

The authors declare no competing financial interests.

ABBREVIATIONS

cAMP – Cyclic adenosine monophosphate

cGMP – Cyclic guanine monophosphate

CNGA1 – Cyclic nucleotide gated channel alpha 1

CNGB1 – Cyclic nucleotide gated channel beta 1

CNTF – Ciliary neurotrophic factor

ERG – Electroretinogram

FASP – Filter-aided sample preparation

GBP2 – Guanylate binding protein 2, interferon-inducible

GCL – Ganglion cell layer

GePS – Genomatix pathway system

GFAP – Glial fibrillary acidic protein

LC – Liquid chromatography

LC-MS/MS – Liquid chromatography tandem mass spectrometry

MS – Mass spectrometry

MVP - Major vault protein

ONL – Outer nuclear layer

PB – Phosphate buffer

PDE6 – Rod-specific cGMP phosphodiesterase

PLBC4 - Phospholipase C, beta 4

PN – Post-natal day

rd1 – Retinal degeneration 1

rd10 – Retinal degeneration 10

ROM1 – Rod outer membrane 1

RP – Retinitis pigmentosa

RRAS - Related RAS Viral (R-Ras) Oncogene Homolog

SLC24A1 - Solute carrier family 24 (Sodium/potassium/calcium exchanger), member 1

STAT – Signal transducer and activator of transcription

VCAM1 – Vascular cell adhesion molecule 1

FIGURE LEGENDS

Figure 1. Vertical sections of wild-type and *rd10* retina demonstrating decrease in photoreceptor number over time. At PN14, the size of the outer nuclear layer (ONL) in wild-type (A) and *rd10* (B) retina is comparable. The size of the wild-type ONL is maintained at PN21 (C) and PN28 (E). In comparison, by PN21 the *rd10* ONL (D) is approximately half the size of the age-matched wild-type, and has been reduced to a single layer of nuclei at PN28 (F). Abbreviations: ONL, outer nuclear layer; OPL, outer plexiform layer; INL, inner nuclear layer; IPL, inner plexiform layer; GCL, ganglion cell layer. Scale bar = 50μm.

Figure 2. Heatmap and tree of hierarchical cluster analysis of PN14, PN21 and PN28 proteins.

Proteins were clustered based on the respective fold change *rd10*/wildtype at each time point. The corresponding heatmap and hierarchical tree is given, with downregulated proteins presented in blue and upregulated proteins in yellow for the respective timepoints. Proteins in the individual clusters which were validated by immunofluorescence, qPCR and/or western blot are given in red.

Figure 3. Interaction map of differentially abundant retinal proteins between wild-type and *rd10* mice at P21 (q<0.05). Protein abbreviations are based on official gene symbols (NCBI Entrez Gene). Upregulated proteins are presented in yellow and downregulated proteins in blue. The nature of the proteins and the individual interactions is given in the legend.

Figure 4. Validation of deregulated protein expression.

(A) GFAP immunoreactivity (green) is present only in the GCL in wild-type mice at PN21. Age-matched *rd10* retina shows increased GFAP labelling in Müller cells extending into the ONL. Abbreviations: ONL, outer nuclear layer; OPL, outer plexiform layer; INL, inner nuclear layer; IPL, inner plexiform layer; GCL, ganglion cell layer. Scale bar = 50µm.

(B) STAT1 labelling is low in the wild-type retina at PN21, and increased in *rd10* retina. At PN21, double labelling of *rd10* retina with STAT1 (green) and glutamine synthetase (GS, red) indicates that STAT1 is increased in Müller cell processes, given by an overlay of green and red coloring resulting in yellow signals. This colocalisation is absent in the wild-type retina. Abbreviations: see (A), Scale bar = 50µm.

(C) The *rd10*/wild-type expression level of genes from different clusters (see figure 2, *Pde6b* for cluster A*, Slc24a1* for cluster B*, Stat1* and *Stat3, Mvp* and *Gfap* for cluster E) was determined by RT-qPCR (gray; error bars represent SEM = standard error of the mean, n=2 for *Stat1*, n=4 for all others) and compared to the respective proteomics data (yellow for upregulated proteins and blue for downregulated proteins). The corresponding primer sequences are given in supplemental table 5.

(D) Western blot showing increases in the levels of STAT1, phospho-STAT1, STAT3, and phospho-STAT3 in comparison to the tubulin loading control in the *rd10* retina.

FIGURES

Figure 1

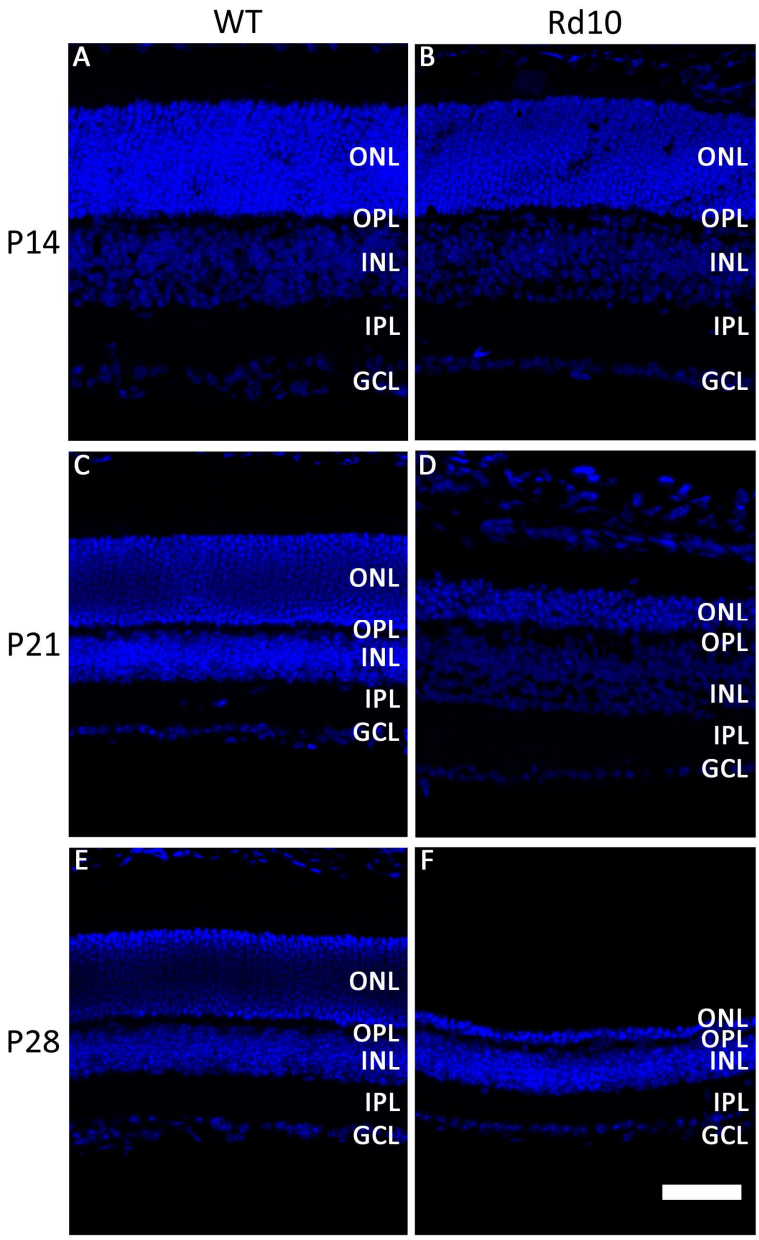

Figure 2

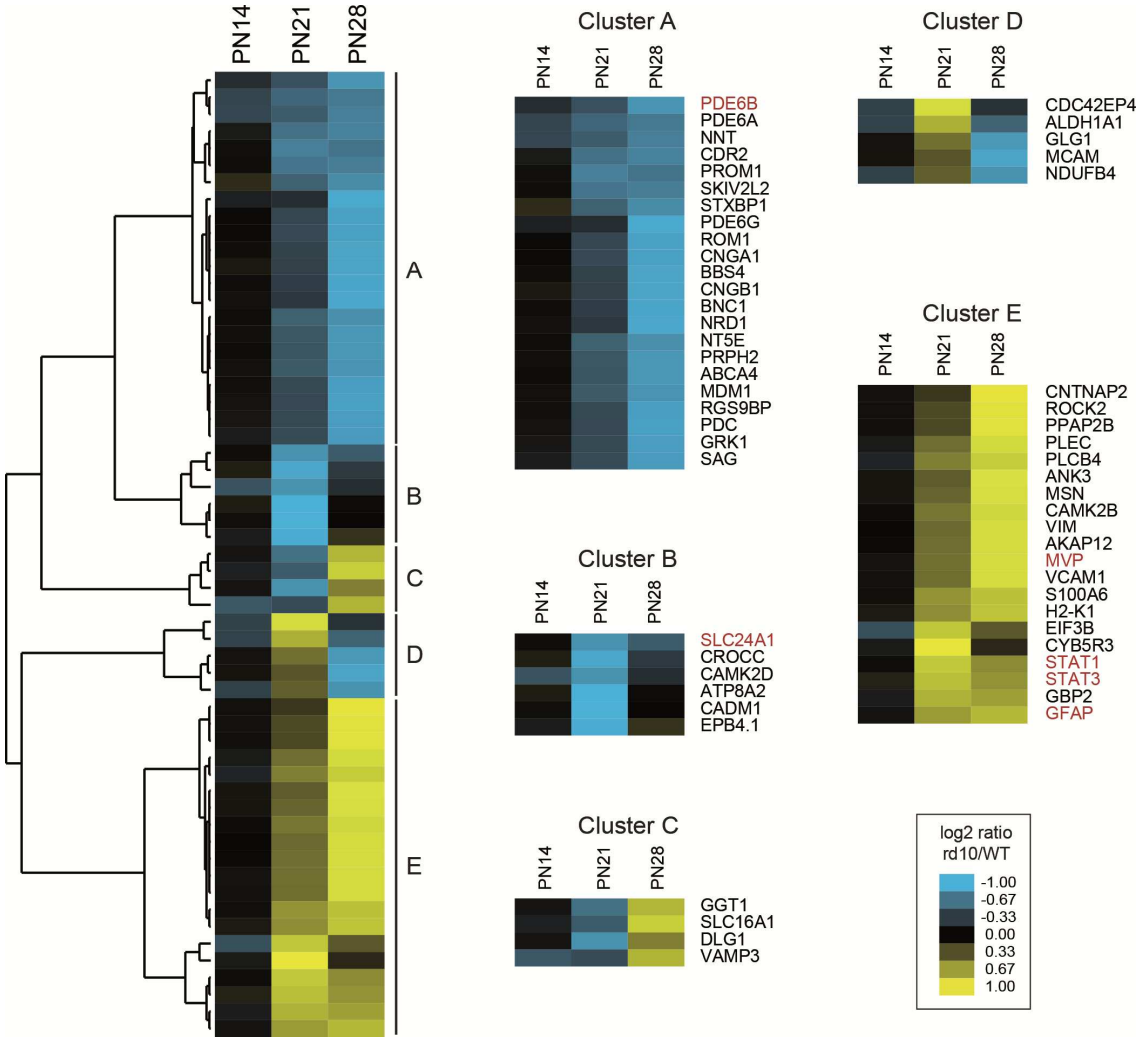
PN14
PN21
PN28
A
B
C
D
E
Cluster A
PDE6B
PDE6A
NNT
CDR2
PROM1
SKIV2L2
STXBP1
PDE6G
ROM1
CNGA1
BBS4
CNGB1
BNC1
NRD1
NT5E
PRPH2
ABCA4
MDM1
RGS9BP
PDC
GRK1
SAG
Cluster B
SLC24A1
CROCC
CAMK2D
ATP8A2
CADM1
EPB4.1
Cluster C
GGT1
SLC16A1
DLG1
VAMP3
Cluster D
CDC42EP4
ALDH1A1
GLG1
MCAM
NDUFB4
Cluster E
CNTNAP2
ROCK2
PPAP2B
PLEC
PLCB4
ANK3
MSN
CAMK2B
VIM
AKAP12
MVP
VCAM1
S100A6
H2-K1
EIF3B
CYB5R3
STAT1
STAT3
GBP2
GFAP
log2 ratio
rd10/WT
-1.00
-0.67
-0.33
0.00
0.33
0.67
1.00

Figure 3

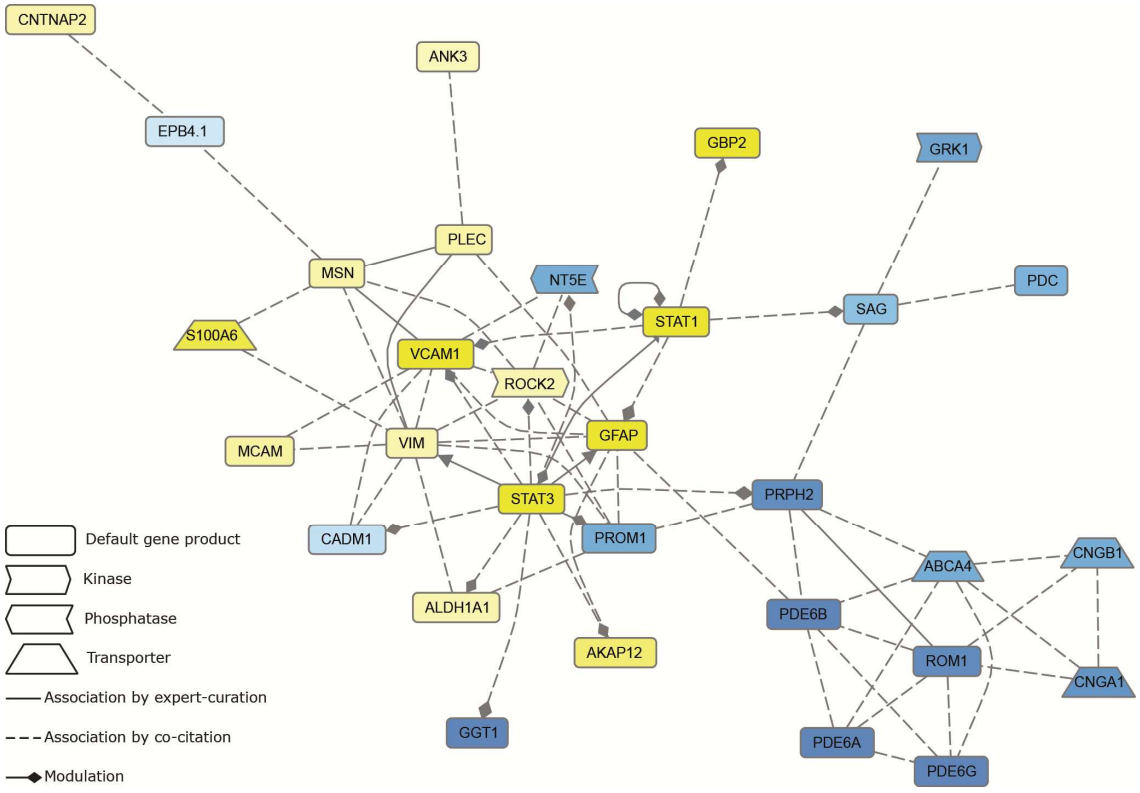
CNTNAP2
ANK3
EPB4.1
GBP2
GRK1
PLEC
MSN
NT5E
PDC
STAT1
SAG
S100A6
VCAM1
ROCK2
GFAP
MCAM
VIM
PRPH2
STAT3
CADM1
PROM1
ABCA4
CNGB1
ALDH1A1
PDE6B
AKAP12
ROM1
CNGA1
GGT1
PDE6A
PDE6G
Default gene product
Kinase
Phosphatase
Transporter
Association by expert-curation
Association by co-citation
Modulation

Figure 4

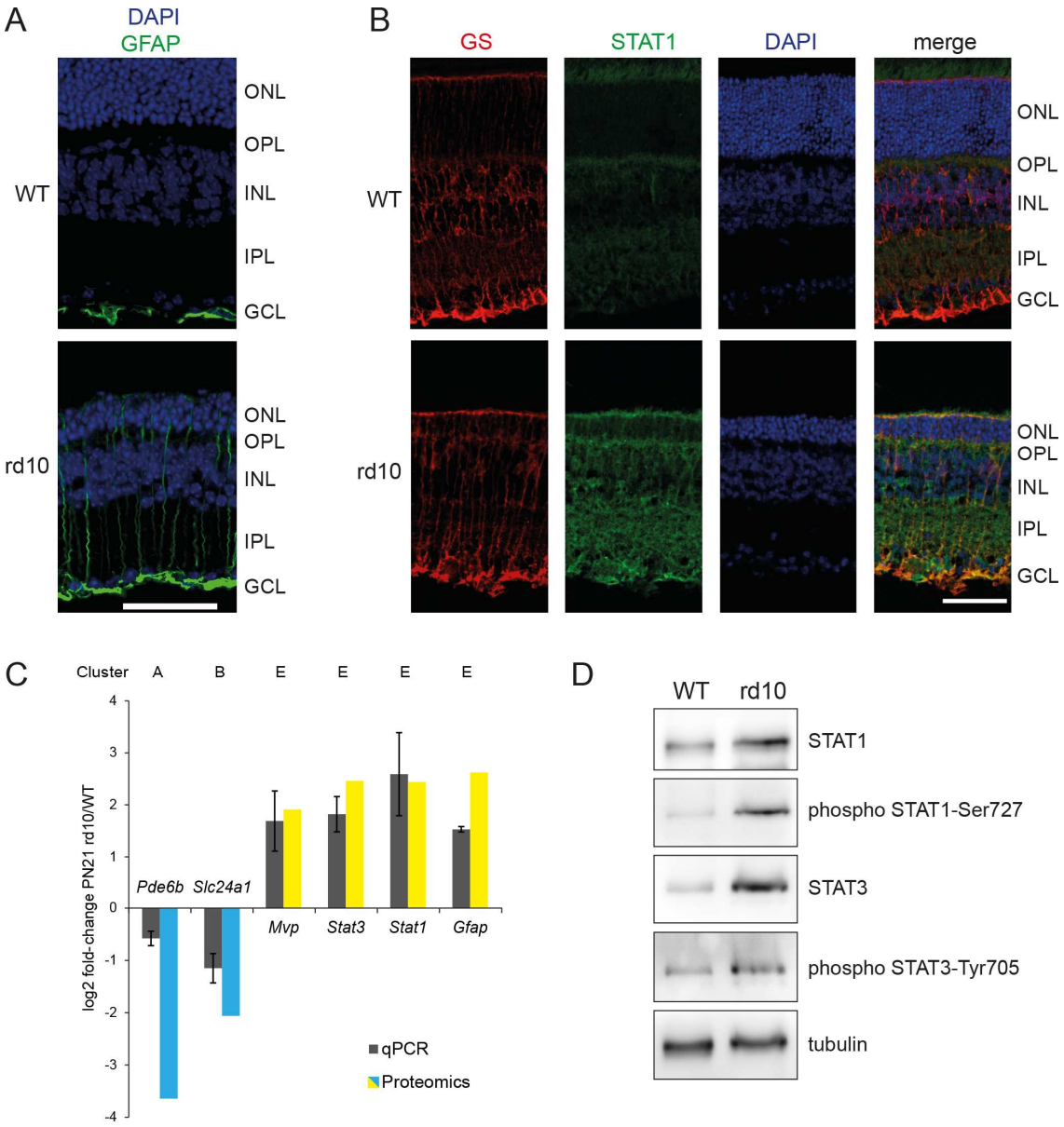
A
DAPI
GFAP
WT
rd10
ONL
OPL
INL
IPL
GCL
B
GS
STAT1
DAPI
merge
WT
rd10
C
Cluster A B E E E E
log2 fold-change PN21 rd10/WT
Pde6b
Slc24a1
Mvp
Stat3
Stat1
Gfap
qPCR
Proteomics
D
WT
rd10
STAT1
phospho STAT1-Ser727
STAT3
phospho STAT3-Tyr705
tubulin

SUPPORTING INFORMATION

Supplemental table 1: Normalized abundances of proteins identified and quantified by LC-MS/MS, with corresponding ratios rd10/WT and significance values

Supplemental table 2: Significantly altered proteins at PN14 with q-value<0.05

Supplemental table 3: Significantly altered proteins at PN21 with q-value<0.05, with corresponding clusters in figure 2

Supplemental table 4: Significantly altered proteins at PN28 with q-value<0.05

Supplemental table 5 Primer sequences for qPCR

Supplemental table 6: Molecular functions overrepresented with clusters A and B with p<0.005

Supplemental table 7: Molecular functions overrepresented with cluster E with p<0.005

Supplemental figure 1 Volcano plot of *rd10* vs wildtype fold changes at PN14 (A, blue), PN21 (B, red), and PN28 (C, green), and the combination of all three time points (D). Protein fold changes are compared to the respective significance values. The negative $\log_{10}$ of the significance *q*-value is plotted against the $\log_2$ of the *rd10*/wild-type fold change.

for TOC only

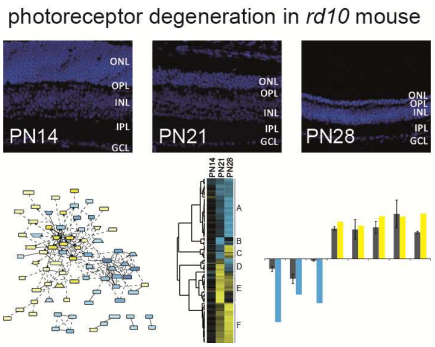
photoreceptor degeneration in *rd10* mouse
ONL
OPL
INL
IPL
GCL
PN14
PN21
PN28
A
B
C
D
E
F